Available online at www.sciencedirect.com

ScienceDirect

journal homepage: www.elsevier.com/locate/he

Accelerate oxygen evolution reaction by adding chemical mediator and utilizing solar energy

Rong He [a], *Quanwen Sun* [a], *Pitchai Thangasamy* [a], *Xinqi Chen* [b], *Yizhi Zhang* [c], *Haiyan Wang* [c], *Hongmei Luo* [a,**], *Xiao-Dong Zhou* [d,***], *Meng Zhou* [a,*]

[a] *Department of Chemical & Materials Engineering, New Mexico State University, Las Cruces, NM, 88003, USA*
[b] *Northwestern University Atomic and Nanoscale Characterization Experimental (NUANCE) Center and Department of Materials Science and Engineering, Northwestern University, Evanston, IL 60208, USA*
[c] *School of Materials Engineering, Purdue University, West Lafayette, IN, 47907, USA*
[d] *Department of Chemical Engineering, Institute for Materials Research and Innovations, University of Louisiana at Lafayette, Lafayette, LA, 70504, USA*

HIGHLIGHTS

- Current density can be increased 10 times by adding glycerol and raising temperatures.
- The OER activity of Co–S/Ni_3S_2@NF is comparable with the performance of IrO_2@NF.
- The Co–S/Ni_3S_2@NF exhibits high catalytic activity and thermal durability for OER.
- GOR is a promising candidate to replace OER in electrolysis.
- The solar energy can be utilized to improve OER in electrochemical water splitting.

GRAPHICAL ABSTRACT

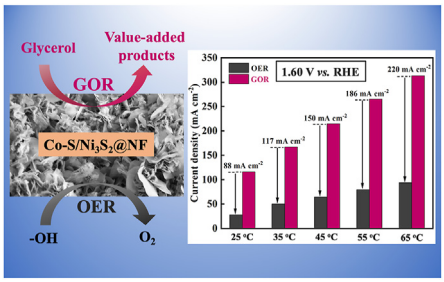

ARTICLE INFO

Article history:
Received 20 September 2022
Received in revised form
17 November 2022
Accepted 26 November 2022
Available online xxx

ABSTRACT

The electrochemical water splitting to produce clean hydrogen is severely restricted by oxygen evolution reaction (OER) due to the sluggish kinetics of its complicated oxidation process. In this work, the cobalt sulfide nanosheets directly grown on nickel foam (Co–S/Ni_3S_2@NF) demonstrated an outstanding OER performance with a potential of 1.57 V (*vs.* RHE) to achieve a current density of 20 mA cm^{-2}, favorably comparing the performance of the noble metal-based catalyst IrO_2@NF. The same current density (20 mA cm^{-2}) could be reached at an extremely low potential of 1.35 V (*vs.* RHE) by adding 0.1 M glycerol, indicating adding chemical mediator is a possible approach to replace the sluggish OER by the

* *Corresponding author.*
** *Corresponding author.*
*** *Corresponding author.*
E-mail addresses: hluo@nmsu.edu (H. Luo), xiao-dong.zhou@louisiana.edu (X.-D. Zhou), mzhou@nmsu.edu (M. Zhou).
https://doi.org/10.1016/j.ijhydene.2022.11.294
0360-3199/Published by Elsevier Ltd on behalf of Hydrogen Energy Publications LLC.

Keywords:
Cobalt sulfide
Oxygen evolution reaction
Glycerol oxidation reaction
Low-grade heat
Thermal durability

corresponding oxidation of chemical mediator. The activation energy comparison of glycerol oxidation reaction (GOR) and OER (21.9 kJ/mol and 28.2 kJ/mol) further proved this conclusion. The solar energy can be captured and utilized to improve OER in the electrochemical water splitting. The anodic current density at ~1.6 V (*vs.* RHE) can be increased 10 times by adding glycerol and raising temperature. This work provides solutions to accelerate OER for H_2 production.

Introduction

New inventions and technologies continuously increase the global energy demand. The rapid energy consumption and the depletion of limited resources such as coal, natural gas, and petroleum have motivated various researchers to exploit renewable and sustainable energy as an alternative [1–5]. Hydrogen has high gravimetric energy density and can be stored and transported, which has attracted significant attention [6]. Electrochemical water splitting is a promising pathway to produce green hydrogen, which plays an essential role in the development of clean and renewable energy conversion and storage [7–10]. Water splitting involves oxygen evolution reaction (OER) and hydrogen evolution reaction (HER) [11,12]. OER is a four-electron transfer process while HER is a two-electron coupled reaction, implying that OER requires a higher overpotential/energy than HER to overcome the sluggish kinetics [13,14]. Hence, the electrocatalytic performance of OER has a significant impact on the overall water splitting rate and energy conversion efficiency [15–17].

Noble metals such as IrO_2 and RuO_2 are highly active toward OER [18–20]. However, the scarcity and high cost of these precious electrocatalysts restrict their large-scale practical application in sustainable energy conversion. Accordingly, various non-noble metal-based materials have been explored as competitive OER electrocatalysts [21–24]. Transition metal oxides, hydroxides, phosphides and chalcogenides have been reported as efficient OER electrocatalysts in water splitting [25–29]. Among them, cobalt-based electrocatalysts have especially attracted great attention over the years due to their abundance, low cost, high OER activity and stability [30,31]. It has been reported that the OER activity of cobalt-based electrocatalysts can be significantly improved by changing the morphology, structure, oxidation states and creating more oxygen vacancies [32–35]. For example, Li et al. synthesized a pre-catalyst P/Mo–Co_3O_4 on carbon cloth for electrochemical OER, which exhibited a low overpotential of 265 mV at 10 mA cm^{-2} for OER [36]. The surface self-reconstruction of Co-PO_4 species and oxygen vacancies on P/Mo–Co_3O_4 provided abundant active sites, making it a promising catalyst for OER. Their results revealed that the Mo doping optimizes adsorption-free energy of *OOH formation, improving the intrinsic electrocatalytic activity.

Despite these advancements in the understanding of cobalt-based electrocatalysts for OER, these cobalt-based materials still suffer from low electrical conductivity and dissolution, and agglomeration during the electrocatalytic reaction, resulting in relatively low energy conversion efficiencies in water splitting [8,37]. To solve these problems, tremendous efforts have been made to develop new strategies to improve OER activity [30,38,39]. One strategy to enhance energy conversion efficiency is seeking an alternative to replace OER as an anodic reaction for hydrogen production by electrolysis [40–42]. Glycerol oxidation reaction (GOR) has been reported as a promising candidate to replace OER, owing to their low thermodynamic potential, and thus decrease the energy consumption for hydrogen production [43,44]. In addition, the price of glycerol is low as it is a by-product derived from the biodiesel and bioethanol production process [45]. Furthermore, glycerol provides a promising pathway to produce high-value-added chemicals including 2-carbon-atom (C_2) and 3-carbon-atom (C_3) organic compounds [46]. Adding glycerol as chemical mediator has attracted growing attention in hydrogen production and noble metal-free materials have been explored as electrocatalysts for GOR [45]. Recently, Brix et al. reported that a higher anodic current density can be obtained by adding glycerol in 1.0 M KOH as electrolyte solutions, indicating that coupling with glycerol oxidation in water splitting is a highly efficient method to improve anodic reaction for hydrogen production [47]. Li et al. described the process of electrocatalytic H_2 production from the acidic aqueous solution of glycerol using manganese oxide as an effective electrocatalyst. In their study, a low potential of 1.36 V (vs. RHE) for the anodic reactions is required to reach a current density of 10 mA cm^{-2} [48].

The temperature is an important factor that has been shown to affect the OER activity by the improvement of its kinetics and the discharge of the adsorbed oxygen species, facilitating the OER process [49,50]. The temperature effect on Co-based catalysts for OER has been investigated by Zhang et al. [51]. They observed that Co_3O_4 exhibited a higher current density than that of noble metal-based oxide (IrO_2) at 65 °C, indicating that temperature plays a critical role in water splitting. The use of low-grade heat sources has attracted more attentions due to increasing energy costs and depleting non-renewable sources [52,53]. Low-grade heat sources such as solar energy has been widely applied in water desalination system and for generating electricity [54,55]. In the water splitting system, the idea to utilize solar energy to heat up the electrolyte solution provides a potential energy-saving approach, speeding up the OER kinetics and thus improving energy efficiency of hydrogen production.

Herein, a cobalt sulfide-based electrocatalyst was fabricated by a simple hydrothermal method. We analyzed the electrochemical performance and stability of prepared cobalt sulfide for anodic reactions in alkaline electrolytes with and without glycerol. Furthermore, we investigated the

Please cite this article as: He R et al., Accelerate oxygen evolution reaction by adding chemical mediator and utilizing solar energy, International Journal of Hydrogen Energy, https://doi.org/10.1016/j.ijhydene.2022.11.294

correlation between temperature and the electrocatalytic activity of the cobalt sulfide for OER and GOR. This paper concentrates on seeking efficient strategies to overcome the slow kinetics of OER, improving the H_2 production efficiency from water electrolysis.

Experimental section

Reagents

Cobalt (II) nitrate hexahydrate ($Co(NO_3)_2 \cdot 6H_2O$), iridium(IV) oxide powder (IrO_2), thiourea, potassium hydroxide (KOH), glycerol, hydrochloric acid (HCl) and acetone were purchased from Sigma-Aldrich. All the mentioned chemicals were of analytical grade and used as received.

Preparation of the electrocatalysts

Conductive Ni foam (NF) as substrate was cut into pieces with dimensions of 2 × 3 cm^2. These NF pieces were cleaned by sonication sequentially in 3 M HCl solution, distilled (DI) water, acetone, and ethanol under sonication to remove oxide layers on the NF surface. The direct growth of cobalt sulfide nanosheets on the NF (Co−S/Ni_3S_2@NF) was performed via a hydrothermal method. At first, 1 mmol $Co(NO_3)_2 \cdot 6H_2O$ and 2 mmol thiourea powder were dissolved in 50 mL DI water, and the resulting mixture solution was transferred to a 100 mL Teflon-lined stainless steel autoclave reactor. Then the pretreated NFs were placed vertically in the above solution and kept in an electric oven, where the temperature of the oven was raised and maintained for 12 h at 120 °C. The prepared Co−S/Ni_3S_2@NF was washed with DI water and ethanol several times and then dried in an oven at 60 °C for 12 h Ni_3S_2@NF was also prepared using the same method without adding cobalt precursor. For the OER activity comparison purpose, a noble metal-based electrocatalyst i.e., IrO_2@NF was also prepared. Simply, 5 mg of IrO_2 powder was dispersed in a solution containing 200 μl of H_2O and 10 μl of Nafion. Then the mixture was kept in an ultrasonic bath for 30 min and the obtained catalyst ink was dropped onto a 1 × 1 cm^2 NF, making a mass loading of ~1.3 mg cm^{-2} which is the same as cobalt sulfide on NF (Co−S/Ni_3S_2@NF).

Characterization techniques

X-ray diffraction (XRD) patterns were obtained from a PANalytical Empyrean powder diffractometer with Cu Ka (λ = 1.5406 Å) with a 2θ range of 10°−80. The microstructure and surface topography of materials were investigated by field emission scanning electron microscopy (FESEM, Tescan Mira3), energy dispersive X-ray spectroscopy (EDS), transmission electron microscopy (TEM, Thermo Fisher Talos F200X microscope) and atomic force microscopy (AFM, BRUKER Dimension FastScan). The composition and surface properties of samples were analyzed by X-ray photoelectron spectroscopy (XPS) using Thermo Fisher ESCALAB 250Xi equipped with an Al kα X-ray source (1486.6 eV). The XPS spectra were calibrated against the carbon (C 1s) peak at 284.80 eV.

Electrochemical measurements

The electrochemical measurements were performed on an electrochemical workstation (CHI 760C) with a potentiostat in a typical three-electrode setup, using prepared NF-based samples (1 × 1 cm^2) as the working electrode, a platinum (Pt) coil as the counter electrode and a silver/silver chloride (Ag/AgCl) electrode as the reference electrode. 1.0 M KOH or 1.0 M KOH with 0.1 M glycerol was used as the alkaline electrolyte solution. The working electrode was cycled at a scan rate of 20 mV s^{-1} for 30 cycles to activate the electrode in the electrolyte and then cyclic voltammograms (CVs) at a scan rate of 10 mV s^{-1} were collected. The polarization curves were obtained by linear sweep voltammetry (LSV) at a scan rate of 5 mV s^{-1}. Electrochemical impedance spectroscopy (EIS) measurements were carried out from 10^5 Hz to 0.1 Hz with potentials of 0.55 V and 0.35 V vs. Ag/AgCl for OER and GOR, respectively. The stability tests were performed by applying a certain constant current in both 1.0 M KOH and 1.0 M KOH with 0.1 M glycerol for 10 h using chronopotentiometry techniques. To investigate the temperature effect on OER and GOR performance, the electrochemical measurements were carried out at a range of temperatures from 25 to 65 °C.

Results and discussion

The cobalt sulfide on Ni foam as the working electrode was prepared through a simple one-step hydrothermal process. A comparison of SEM images of bare Ni foam, Ni_3S_2@NF and Co−S/Ni_3S_2@NF samples is shown in Fig. 1. As can be observed, bare Ni foam presents a 3-dimensional (3D) porous morphology and has a smooth surface as displayed in the high-magnification images (Fig. 1a and b). SEM images of Ni_3S_2@NF reveal that dense nickel sulfide nano particles grown on Ni foam surface (Fig. 1c and d). In addition, the corresponding elemental mappings confirmed the uniform distribution of Ni and S in the particles (Fig. S1). Hydrothermal synthesis of CoS_x on the Ni foam was achieved using Co^{2+} precursor solution and thiourea as sulfide precursor reacting with Ni form. The color of the Ni foam surface changed to green after the hydrothermal reaction. The rough surface of Ni foam was also observed, indicating the successful growth of CoS_x nanostructures on the Ni foam (Fig. 1e). The high-magnification SEM image (Fig. 1f) further reveals that CoS_x has a sheet-like morphology that is uniformly anchored on the surface of Ni foam, leading to the formation of robust electrocatalyst for the OER and GOR. The corresponding elemental mappings demonstrate that Co, S, and Ni elements uniformly distribute in the Co−S/Ni_3S_2@NF (Fig. 1g–j). The composition of Co−S/Ni_3S_2@NF was further examined by TEM. The elements of Co, Ni and S were uniformly distributed in the nanosheets of Co−S/Ni_3S_2@NF, further indicating the formation of cobalt - nickel sulfides on the NF surface (Fig. S2).

The structures of the prepared materials were primarily analyzed by XRD. The XRD patterns of bare NF, Ni_3S_2@NF, and Co−S/Ni_3S_2@NF in Fig. 2a show three characteristic diffraction peaks of nickel, which come from the Ni foam substrate. In Fig. 2b, the diffraction peaks of Ni_3S_2@NF at 22.5, 31.8, 38.3, 50.5, and 55.3° correspond respectively to the (101), (110), (003),

Please cite this article as: He R et al., Accelerate oxygen evolution reaction by adding chemical mediator and utilizing solar energy, International Journal of Hydrogen Energy, https://doi.org/10.1016/j.ijhydene.2022.11.294

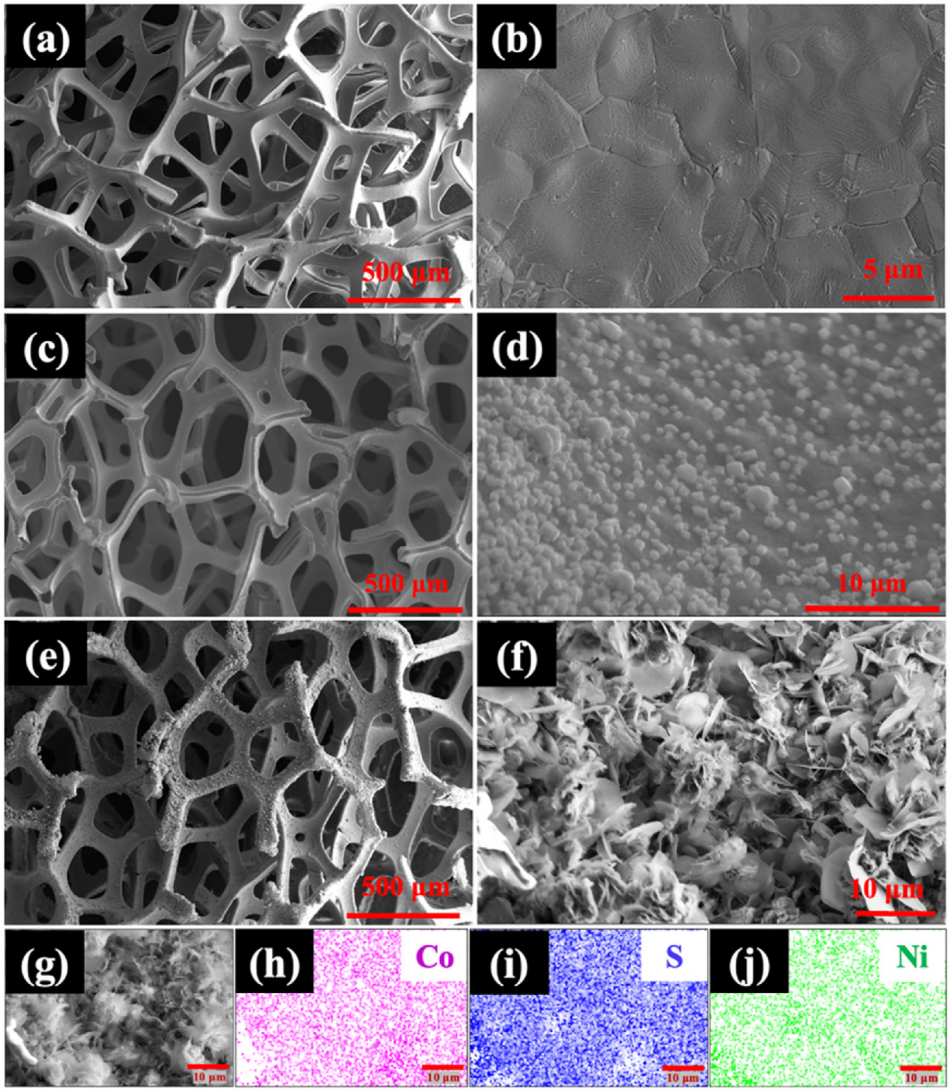

Fig. 1 – SEM images of (a, b) bare NF, (c, d) Ni_3S_2@NF and (e, f) Co–S/Ni_3S_2@NF samples, and (g–j) energy dispersive spectrometry (EDS) mapping analysis of Co–S/Ni_3S_2@NF.

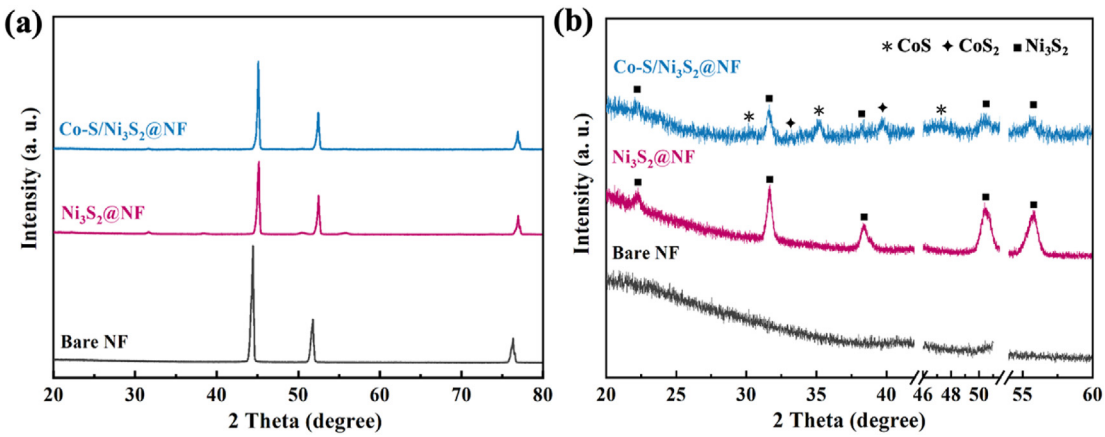

Fig. 2 – (a) XRD patterns and (b) the magnified patterns of bare NF, Ni_3S_2@NF and Co–S/Ni_3S_2@NF.

Please cite this article as: He R et al., Accelerate oxygen evolution reaction by adding chemical mediator and utilizing solar energy, International Journal of Hydrogen Energy, https://doi.org/10.1016/j.ijhydene.2022.11.294

(113), and (122) planes of Ni_3S_2 (JCPDS No. 44-1418), which are the products of the sulfurization of Ni foam [56]. These peaks were also observed in the XRD pattern of Co–S/Ni_3S_2@NF, indicating that thiourea undergoes decomposition followed by the reaction with cobalt metal atoms as well as Ni foam substrate during the hydrothermal reaction. Co–S/Ni_3S_2@NF exhibit the diffraction peaks corresponding to the CoS (JCPDS No. 75-0605) and CoS_2 (JCPDS No. 41-1471) diffraction peaks [57]. This result indicates that cobalt sulfide nanosheets with different phases/compositions were successfully grown on Ni foam by a facile hydrothermal process.

The surface properties and chemical composition of Co–S/Ni_3S_2@NF were also examined by XPS. The wide scan XPS survey spectra of Co–S/Ni_3S_2@NF confirmed the existence of Co, Ni, S, C, N, and O elements (Fig. 3a). In the high-resolution Co 2p spectrum (Fig. 3b), the two main peaks centered at 781.6 eV (Co $2p_{3/2}$) and 797.2 eV (Co $2p_{1/2}$) with their neighboring shakeup satellite peaks can be identified as characteristic peaks of Co species with +2 oxidation state, indicating that the formation of CoS and CoS_2 in Co–S compounds [58]. The binding energies at 161.43, 162.5, 163.3, and 164.6 eV correspond to S^{2-} $2p_{3/2}$, S^{2-} $2p_{1/2}$, S_2^{2-} $2p_{3/2}$ and S_2^{2-} $2p_{1/2}$, respectively (Fig. 3c) [59]. The peak at ~168.6 eV is related to the oxidized S species containing sulfate or sulfite groups (SO_x^{n-}), which is most likely from the possible oxidation of S under hydrothermal conditions [59]. The Ni 2p spectrum is split into two spin-orbit doublets and two shake-up satellites (Fig. 3d). Two characteristic peaks appeared at 856.3 and 873.9 eV, which can be ascribed to the Ni $2p_{3/2}$ and Ni $2p_{1/2}$ peaks related to Ni species in Ni_3S_2 [60,61]. All the XPS observations demonstrate the successful synthesis of cobalt sulfides containing CoS and CoS_2 on Ni foam after the hydrothermal reaction, which is consistent with the XRD analysis.

To evaluate the catalytic performance of the prepared working electrode, the catalytic properties of the fabricated electrocatalysts toward OER and GOR were measured in 1.0 M KOH or 1.0 M KOH with 0.1 M glycerol electrolyte solutions. As shown in the LSV curves (Fig. 4a), the Co–S/Ni_3S_2@NF electrode exhibits much higher catalytic activity toward OER demanding an overpotential of ~340 mV to reach 20 mA cm^{-2}, which is superior to the bare Ni foam (~2.3 mA cm^{-2} at an overpotential of 340 mV) and comparable with the noble metal-based electrode (IrO_2@NF). The prepared hybrid electrocatalyst (Co–S/Ni_3S_2@NF) in this work would possess the following advantages: firstly, this electrocatalyst has good conductivity resulting from the Ni foam substrate, which is beneficial for charge transfer and thus improves the electrochemical performance; secondly, the high porosity structure of Ni foam provides a large surface area for the active materials, cobalt sulfide in this case, which will lead to the exposure of abundant active sites for the catalytic reactions and finally, Co–S/Ni_3S_2@NF has a unique 3D structure from Ni

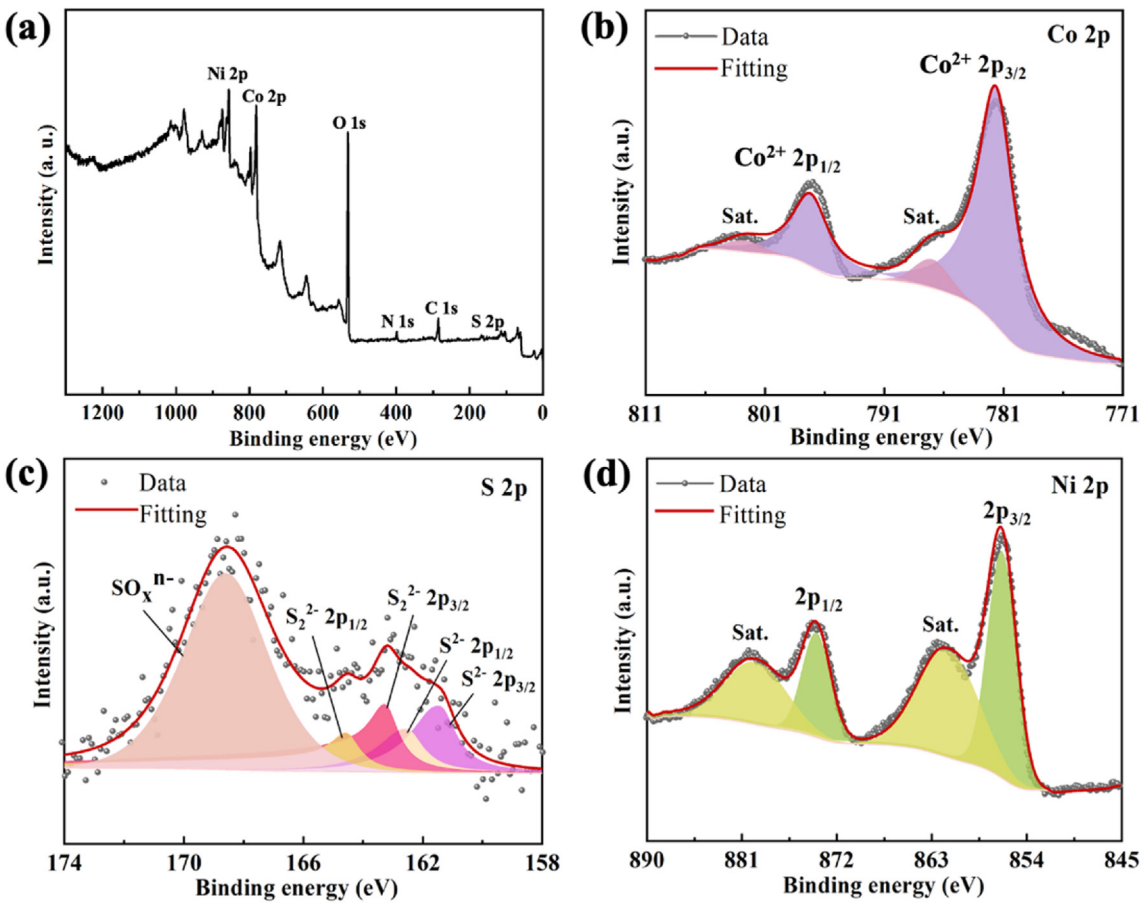

Fig. 3 – (a) XPS survey spectrum of the Co–S/Ni_3S_2@NF, and their corresponding high-resolution spectra (b) Co 2p, (c) S 2p and (d) Ni 2p.

Please cite this article as: He R et al., Accelerate oxygen evolution reaction by adding chemical mediator and utilizing solar energy, International Journal of Hydrogen Energy, https://doi.org/10.1016/j.ijhydene.2022.11.294

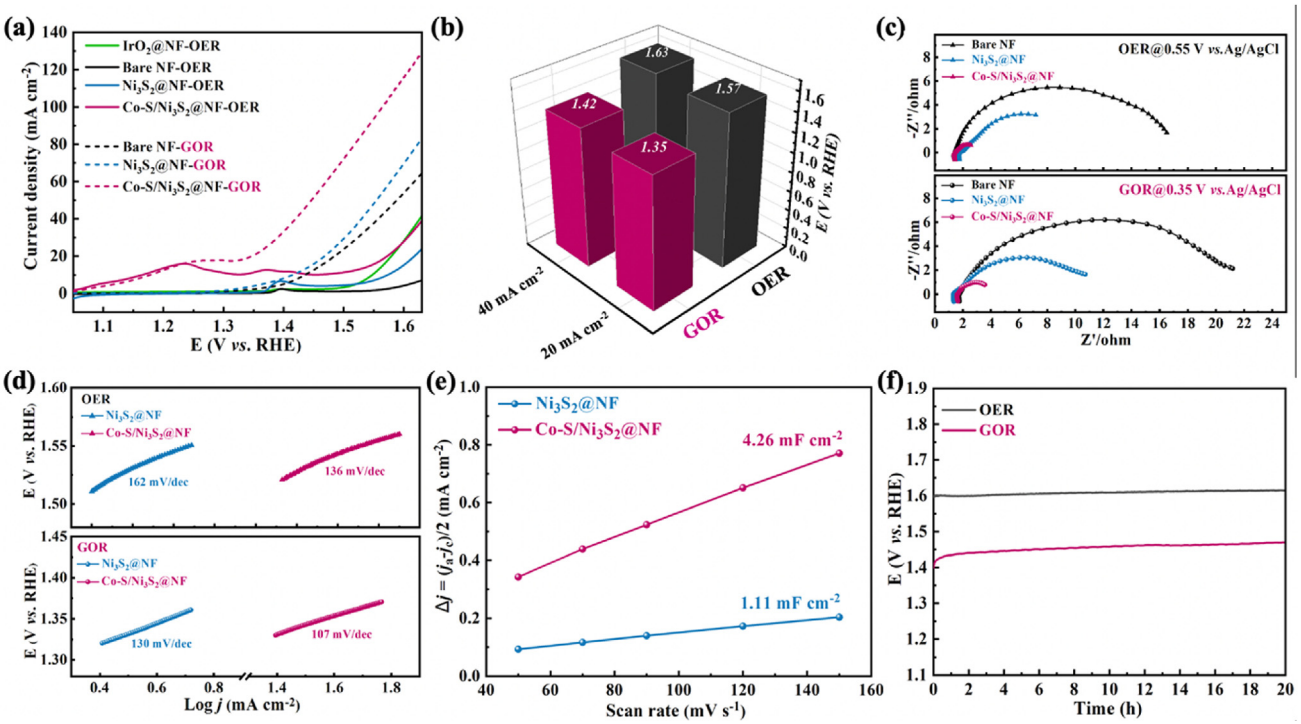

Fig. 4 – (a) LSV curves of the different electrocatalysts measured in 1.0 M KOH and 1.0 M KOH with 0.1 M glycerol, at a scan rate of 5 mV s^{-1}; (b) 3D histogram comparing the potentials of Co–S/Ni_3S_2@NF for OER and GOR; (c) Electrochemical impedance spectra of the different electrocatalysts at the applied potentials of 0.55 and 0.35 V (*vs.* Ag/AgCl) for the OER and GOR, respectively; (d) Tafel plots of Ni_3S_2@NF and Co–S/Ni_3S_2@NF for OER and GOR; (e) Current density as a function of the scan rates for Ni_3S_2@NF and Co–S/Ni_3S_2@NF; (f) Stability testing of Co–S/Ni_3S_2@NF for OER and GOR under a constant current density of 30 mA cm^{-2}.

foam, which facilitates the exchange of absorbed reactants and the release of oxygen. It is worth mentioning that Ni_3S_2@NF shows higher OER and GOR activities than bare NF, which means that nickel sulfides also contribute to the catalytic activity towards OER and GOR. Hence, we can reasonably conclude that the high OER and GOR activities of Co–S/Ni_3S_2@NF is due to the synergistic effect of Ni foam, cobalt sulfides, and nickel sulfides. Impressively, this Co–S/Ni_3S_2@NF electrode only requires a potential of 1.35 V *vs.* RHE to deliver a current density of 20 mA cm^{-2} in 1.0 M KOH with 0.1 M glycerol, which displays superior GOR activity. Fig. 4b shows the comparison of potentials for OER and GOR at current densities of 20 and 40 mA cm^{-2}. The potential for anodic oxidation decreased by 220 mV and 210 mV to reach the current densities of 20 and 40 mA cm^{-2}, respectively, by adding 0.1 M glycerol. This result demonstrated that GOR was more conducive than OER to occurring at a low potential. Glycerol can be converted into value-added products. Basically, during the GOR process, the –OH groups of glycerol can be oxidized to produce different products depending on the catalytic activity and selectivity of the materials [62]. The most common products of GOR are 3-carbon-atom compounds (e.g., glyceraldehyde and dihydroxyacetone) and 2-carbon-atom compounds (e.g., glyoxylic acid and oxalic acid). CO_2 is difficult to generate due to the slow kinetics and high energy barrier for breaking both C–C bonds in glycerol [45]. It is known that non-precious transition metals like Ni and Co-based electrocatalysts have been widely investigated due to their low cost and high electrocatalytic activity toward GOR [63]. Some studies of transition metal-based electrocatalysts for OER and GOR are summarized in Table 1. Cechanaviciute et al. synthesized a series of multi-metal electrocatalysts for OER and GOR [64]. Their results also showed that GOR requires a lower potential to reach the same current density compared to OER.

Table 1 – Comparison of OER and GOR performance of different catalysts reported in the literature.

Catalysts	OER potential (V *vs.* RHE)	GOR potential (V *vs.* RHE)	Sample preparation method	References
$Co_{20}Cu_{20}Ni_{20}Ag_{20}Zn_{20}$	~1.67 @ 20 mA cm^{-2}	1.50 @ 17 mA cm^{-2}	Aerosol-based synthesis	Cechanaviciute et al. [64]
CoNiCuMnMo-NPs/CC	1.55 @ 10 mA cm^{-2}	1.25 @ 10 mA cm^{-2}	Pyrolysis reduction	Fan et al. [65]
$LaFe_{0.31}Co_{0.69}O_3$	~1.65 @ 10 mA cm^{-2}	1.60 @ 10 mA cm^{-2}	Co-precipitation	Brix et al. [47]
Co–S/Ni_3S_2@NF	1.57 @ 20 mA cm^{-2}	1.35 @ 20 mA cm^{-2}	Hydrothermal method	**This work**

Please cite this article as: He R et al., Accelerate oxygen evolution reaction by adding chemical mediator and utilizing solar energy, International Journal of Hydrogen Energy, https://doi.org/10.1016/j.ijhydene.2022.11.294

However, the electrocatalysts contain five metals ($Co_{20}Cu_{20}Ni_{20}Ag_{20}Zn_{20}$), which is complicated, and the current density is relatively low (17 mA cm^{-2} at 1.5 V *vs.* RHE) [64]. Recently, Fan et al. measured the overall potentials for HER-OER and HER-GOR electrolyzers [65]. They found that an applied voltage of 1.55 V *vs.* RHE is required to deliver a current density of 10 mA cm^{-2} for a conventional cell using 1 M KOH as electrolyte while only 1.25 V *vs.* RHE is required to achieve the same current density by adding 0.1 M glycerol. These previous findings along with our experimental results demonstrate that GOR is a promising candidate to replace OER at an electrolytic anode. It is also reported that the conductivity and chemical stability of the electrocatalysts are important factors for GOR [62]. In this study, the prepared Co–S/Ni_3S_2@NF exhibits excellent electrocatalytic performance for GOR can be attributed to the 3D structure of Ni foam and the uniform distribution of cobalt -nickel sulfides, which improve the electrocatalyst conductivity and provide abundant accessible active sites.

The electrochemical behavior of as-synthesized Co–S/Ni_3S_2@NF towards OER and GOR has been investigated by cyclic voltammetry and shown in Fig. S3. For OER, Co–S/Ni_3S_2@NF exhibited a strong oxidation peak at ~1.24 V (*vs.* RHE), which is due to the oxidation of Co^{2+} to $Co^{3+/4+}$ [66]. In addition, the anodic peak observed at ~1.37 V (*vs.* RHE) corresponds to the oxidation of Ni^{2+} to Ni^{3+} [67]. The cobalt oxidation was also observed in the CV curve for GOR, which is located at ~1.30 V (*vs.* RHE). The kinetics of the electrocatalytic processes were examined by EIS to further illustrate the OER and GOR activities on Co–S/Ni_3S_2@NF (Fig. 4c). The EIS spectra for OER and GOR were recorded at 0.55 V and 0.35 V (*vs.* Ag/AgCl), respectively. Compared to bare NF and Ni_3S_2@NF, the Co–S/Ni_3S_2@NF has the lowest charge-transfer resistance in OER and GOR, indicating the superior charge transport kinetics due to the higher electronic conductivity at the Co–S/Ni_3S_2@NF electrode/electrolyte interface during the electrochemical reactions. Tafel slopes can be used to indicate the rate of change of potential with the log of current density. Fig. 4d shows the Tafel plots of Ni_3S_2@NF and Co–S/Ni_3S_2@NF for OER and GOR. Tafel slopes of Co–S/Ni_3S_2@NF were found to be 136 mV dec^{-1} for OER, which is lower than that of Ni_3S_2@NF (162 mV dec^{-1}). This means that Co–S/Ni_3S_2@NF is more favorable reaction kinetics toward OER than Ni_3S_2@NF. The high Tafel slopes of Ni_3S_2@NF and Co–S/Ni_3S_2@NF imply that the rate-determining step for OER is probably the M–OH bond formation (M: active sites) [68]. Furthermore, the Co–S/Ni_3S_2@NF has a smaller slope of 107 mV dec^{-1} for GOR than for OER (136 mV dec^{-1}), indicating the faster catalytic kinetics of GOR. The double layer capacitance (C_{dl}) of a catalyst is strongly correlated to its electrochemical activity. The C_{dl} value was obtained from the slope of the linear fitting between the current density differences ($\Delta j = (j_a - j_c)/2$) *vs.* the scan rates from CV curves in the non-Faradic region (Fig. S4). As shown in Fig. 4e, Co–S/Ni_3S_2@NF (4.26 mF cm^{-2}) presents a higher C_{dl} than Ni_3S_2@NF (1.11 mF cm^{-2}). This result indicates that Co–S/Ni_3S_2@NF can provide larger electrochemical active surface area (ECSA) and more accessible active sites than Ni_3S_2@NF during OER and GOR. The above findings demonstrate that adding glycerol as chemical mediator can help to reach a higher current density in KOH electrolyte. Firstly, the glycerol has a lower theoretical oxidation potential and thus GOR will take place before OER, reducing the electricity consumption of the overall electrolysis process. Secondly, the oxidation products of glycerol could be C_3 compounds by oxidizing –OH groups of glycerol and C_2/C_1 compounds by breaking its C–C bonds [44]. GOR as an anodic reaction could be coupled with HER as a cathodic reaction in an electrolysis cell to produce H_2 on the cathode and value-added organic chemicals instead of O_2 on the anode, which can increase the economic value of the electrolysis process. In addition, GOR has a faster reaction kinetics than OER. Therefore, GOR could be a promising candidate to replace OER in an electrolysis cell for hydrogen production.

The electrochemical durability is a significant performance parameter in evaluating the long-term catalytic activity of the electrocatalysts. As shown in Fig. 4f, the chronoamperometric response test of Co–S/Ni_3S_2@NF was conducted in 1.0 M KOH and 1.0 M KOH with 0.1 M glycerol at a constant current density of 30 mA cm^{-2} at room temperature. A stable voltage of about 1.61 V (*vs.* RHE) was sustained for 20 h with negligible degradation for OER. This high stability of Co–S/Ni_3S_2@NF is evidence that this electrocatalyst easily facilities electron transfer and can remain highly active for water oxidation for a long time. The potential of GOR was slightly increased after 20 h of durability test in the Co–S/Ni_3S_2@NF electrode. It is important to note that the potential was increased in the first 2 h and then stabilized in the long-term stability testing. It was reported that the increase in the potential is attributed to the consumption of H^+, OH^-, and glycerol in the electrolyte solution and the potential could be restored to some extent by refreshing the electrolyte [65].

To explore the morphology and composition evolution of the electrocatalyst after electrochemical measurements, the sample Co–S/Ni_3S_2@NF after OER and GOR stability testing was characterized by SEM, XRD and AFM analysis. As displayed in Figs. S5a–b, the Co–S/Ni_3S_2@NF surface showed obvious change after OER testing, which is most likely due to the reconstruction of the catalytically active layer based on cobalt – nickel sulfides during the OER process. The EDS mappings confirmed the existence of Co, Ni, S, O and K elements in Co–S/Ni_3S_2@NF after OER testing (Figs. S5c–h). Potassium was observed in Co–S/Ni_3S_2@NF after OER testing, which was from the electrolyte solution. Moreover, the decrease in cobalt sulfides in the tested Co–S/Ni_3S_2@NF was determined from its XRD patterns as the XRD peaks of CoS and CoS_2 disappeared in the Co–S/Ni_3S_2@NF after OER (Fig. S6). These results may imply that the cobalt sulfide-based active sites readily undergo self-transformation to form true catalytically active sites, which mostly consist of an amorphous layer during the OER stability testing, which was further supported by AFM analysis. It can be clearly seen in Fig. S7 that the Co–S/Ni_3S_2@NF has a rough surface, resulting from the formation of cobalt - nickel sulfides, and the evolution of electrode surface after OER can be observed. The SEM and EDS images of the Co–S/Ni_3S_2@NF after GOR testing indicated that the electrode surface was also reconstructed during GOR process, which is similar to the Co–S/Ni_3S_2@NF after OER testing (Fig. S8). Also, the XRD patterns of Co–S/Ni_3S_2@NF after GOR do not show the peaks for CoS and CoS_2 (Fig. S6). Alike to OER, the catalytic layer of cobalt - nickel sulfides on

Please cite this article as: He R et al., Accelerate oxygen evolution reaction by adding chemical mediator and utilizing solar energy, International Journal of Hydrogen Energy, https://doi.org/10.1016/j.ijhydene.2022.11.294

the NF surface was readily oxidized under an alkaline conditions during the electrochemical reactions, resulting in the surface reconstruction of the Co–S/Ni_3S_2@NF [26]. Based on the above analysis, we can reasonably conclude that cobalt–nickel sulfides were served as the catalytically active layers for both OER and GOR. As we mentioned before, glycerol could be oxidized to various products mainly including C_2/C_3 compounds. The current density increased after adding glycerol, which is most likely because cobalt–nickel sulfides active layers can oxidize the –OH groups of glycerol and cleave its C–C bonds more easily than oxidizing –OH from electrolyte to O_2 (OER).

Raising the operating temperature could be another way to reduce the potential for anodic reactions in an electrolysis cell. According to Arrhenius' law, the reaction rate is related to the temperature [69,70]. Exploring the effect of temperature on anodic reactions can help to understand the electrocatalytic activity of the electrode and the underlying mechanism and thus can guide the future direction in electrocatalyst design. Fig. 5a displays the 3D surface graph showing the effect of temperature on OER performance of Co–S/Ni_3S_2@NF measured in 1.0 M KOH, where the temperature range is from 25 to 65 °C. Interestingly, the anodic current density was significantly increased when the temperature increased from 25 to 65 °C due to the lowering of the activation energy barrier with increasing temperature. It is worth noting that Co–S/Ni_3S_2@NF exhibited better OER performance than IrO_2@NF when the temperature increased to 35 °C, corresponding to the higher OER activity of Co–S/Ni_3S_2@NF at a higher temperature. According to the literature, the possible OER catalytic process over the metal sulfide catalysts in alkaline solutions can be expressed by the equations below, where M refers to active sites [25,71].

$$M + OH^- \rightarrow MOH + e^- \quad (1)$$

$$MOH + OH^- \rightarrow MO^- + H_2O \quad (2)$$

$$MO^- \rightarrow MO + e^- \quad (3)$$

$$MO + MO \rightarrow M + M + O_2 \quad (4)$$

It is generally accepted that the first step (adsorption) of OER is most likely the rate-determining step at room temperature [25]. Zhang et al. have provided a comprehensive study on temperature-dependent OER and suggested that the rate-determining step shifts toward the O–H bond breaking (Eq. (2)) from OH^- adsorption (Eq. (1)) at a higher temperature [51]. This illustrates that a higher current density is obtained as the O–H bond is easier to break at a high temperature. As a comparison in Fig. 5b, it is clearly seen that increasing temperature from 25 to 65 °C results in a monotonically increase in current density for GOR. This result indicates the significant

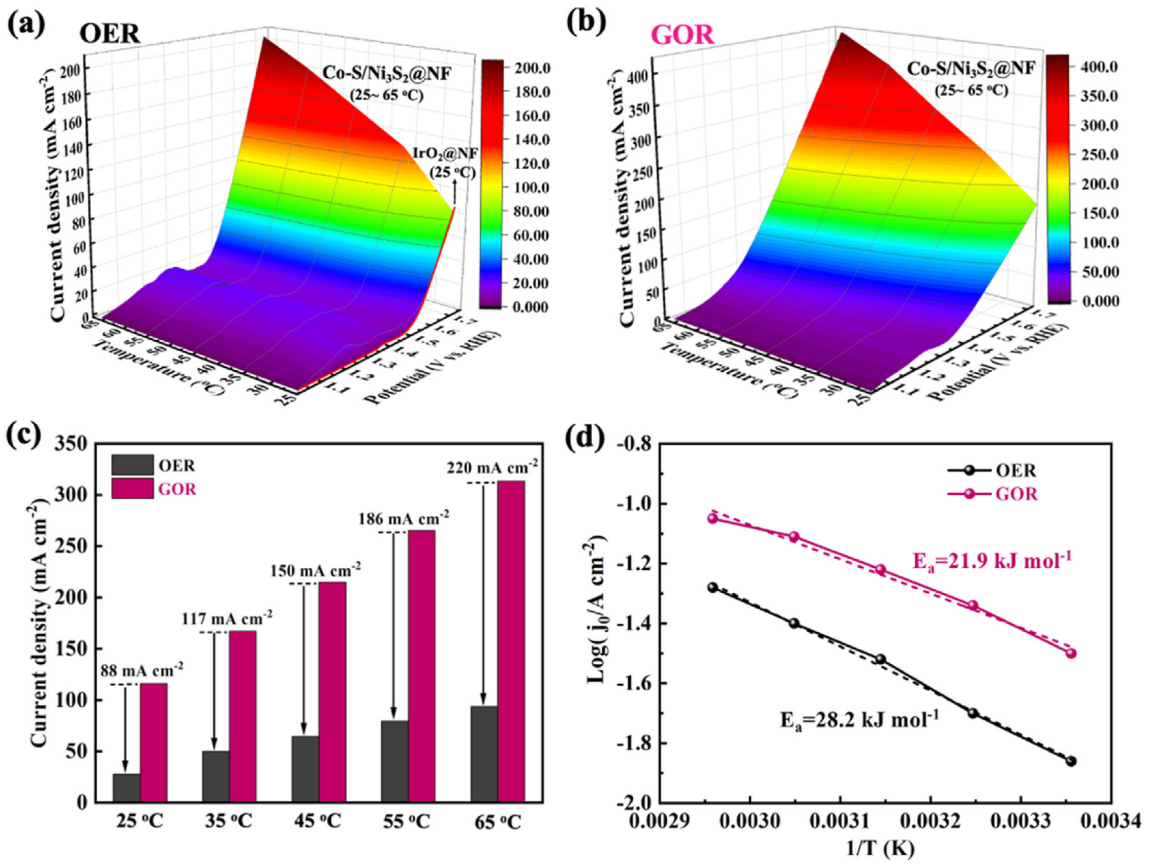

Fig. 5 – The 3D surface graphs showing the effect of temperature on current density *vs.* potential for (a) OER and (b) GOR over Co–S/Ni_3S_2@NF, where the data is obtained from LSV; (c) Comparison of potential for OER and GOR against temperature at 1.60 V *vs.* RHE; (d) Arrhenius plots and calculated activation energies for Co–S/Ni_3S_2@NF for OER and GOR.

Please cite this article as: He R et al., Accelerate oxygen evolution reaction by adding chemical mediator and utilizing solar energy, International Journal of Hydrogen Energy, https://doi.org/10.1016/j.ijhydene.2022.11.294

influence of temperature on glycerol oxidation on Co–S/Ni_3S_2@NF. The increase rate of the OER and GOR with increasing temperature is revealed from the difference in current density between OER and GOR at a certain potential. For example, Fig. 5c compares the current densities between OER and GOR at an applied potential of 1.60 V *vs*. RHE at different temperatures. At 25 °C, the difference in current density between OER and GOR is 88 mA cm^{-2} while this difference increased to 220 at mA cm^{-2} at 65 °C. We can strongly conclude that the temperature is an essential factor to improve the electrocatalytic activity toward the anodic reactions in an electrolysis cell and we found that GOR catalytic activity is more sensitive to temperature compared with OER. Therefore, increasing the temperature for GOR could be an efficient strategy to reduce the potential for anodic reactions for hydrogen generation in an electrolysis cell. It is worth mentioning that the anodic current density at ~1.6 V (*vs*. RHE) increased tenfold in the alkaline electrolysis cell the by adding glycerol and utilizing free solar energy, providing guidance for the development of energy-saving H_2 production systems.

To provide a better understanding of the electrocatalytic behavior, the electrochemical activation energy Ea of OER/GOR for the electrocatalyst was estimated using the temperature-dependent polarization curves based on the Arrhenius assumption [72]. As indicated in Fig. 5d, the calculated Ea value of Co–S/Ni_3S_2@NF for OER is 28.2 kJ mol^{-1}, higher than the value of that for GOR (21.9 kJ mol^{-1}). This observation on activation energy reveals lower reaction barriers involved in the GOR process than OER.

Solar energy could be utilized to produce hydrogen from water splitting by heating it to high temperatures to drive the decomposition of H_2O into H_2 and O_2, a renewable H_2 production pathway [73]. The idea of energy-saving provides a promising future direction for hydrogen production, and this approach may likely be implemented in areas with abundant and strong sunlight. Solar energy has the potential to be used to heat up the electrolyte solution, improving the kinetics of OER/GOR, which might be an effective way to address our energy needs and reduce the energy consumption for the electrolysis system. Thanks to the abundant strong sunlight in New Mexico state, United States, we were able to utilize the solar power to increase the temperature of electrolyte by concentrating sunlight using thermal flasks. The setup of the solar energy collection is shown in Fig. S9.

Conclusions

Developing low-cost efficient electrocatalysts for OER is still a challenging task. In this study, we reported two strategies to improve the OER activity of the cobalt sulfide electrocatalyst for water splitting: adding glycerol to the KOH electrolyte and increasing the temperature. At first, the cobalt sulfide nanosheets grown on nickel foam (Co–S/Ni_3S_2@NF) were successfully synthesized by a simple one-step hydrothermal method. Impressively, this Co–S/Ni_3S_2@NF can afford 20 mA cm^{-2} at a potential of 1.35 V in 1.0 M KOH by adding 0.1 M glycerol as chemical mediator, which is 220 mV lower than OER in 1.0 M KOH. The estimated activation energy of Co–S/Ni_3S_2@NF for OER is higher than that for GOR, indicating the OER process associated with high kinetic energy barriers. Moreover, the electrolyte solution in the electrolysis cell can be heated up utilizing solar energy. By adding glycerol and capturing the solar energy, the anodic current density at ~1.6 V was observed to be increased tenfold in the alkaline electrolysis cell using Co–S/Ni_3S_2@NF as the electrocatalyst. Clearly, we established a link between the temperature and OER/GOR performance and indicated that increasing temperature is an efficient way to improve OER/GOR activity. Furthermore, this Co–S/Ni_3S_2@NF electrocatalyst exhibited high thermal durability. We believe that these findings can provide valuable clues to overcoming the sluggish kinetics of OER process and push the electrochemical activity of OER to the next stage.

Declaration of competing interest

The authors declare that they have no known competing financial interests or personal relationships that could have appeared to influence the work reported in this paper.

Acknowledgments

The work is supported by the National Science Foundation, United States (OIA-2119688).

Appendix A. Supplementary data

Supplementary data to this article can be found online at https://doi.org/10.1016/j.ijhydene.2022.11.294.

REFERENCES

[1] Ulucak R, Danish, Ozcan B. Relationship between energy consumption and environmental sustainability in OECD countries: the role of natural resources rents. Resour Pol 2020;69:101803.
[2] Xie J, Liu W, Zhang X, Guo Y, Gao L, Lei F, et al. Constructing hierarchical wire-on-sheet nanoarrays in phase-regulated cerium-doped nickel hydroxide for promoted urea electrooxidation. ACS Mater Lett 2019;1:103–10.
[3] Zhang L, Liang J, Yue L, Dong K, Li J, Zhao D, et al. Benzoate anions-intercalated NiFe-layered double hydroxide nanosheet array with enhanced stability for electrochemical seawater oxidation. Nano Res Energy 2022;1:e9120028.
[4] Gao L, Xie J, Liu S, Lou S, Wei Z, Zhu X, et al. Crystalline cobalt/amorphous LaCoOx hybrid nanoparticles embedded in porous nitrogen-doped carbon as efficient electrocatalysts for hydrazine-assisted hydrogen production. ACS Appl Mater Interfaces 2020;12:24701–9.
[5] Li J, Dong C, Guo M, Gao W, Kang L, Lei F, et al. Cerium-induced lattice disordering in Co-based nanocatalysts promoting the hydrazine electro-oxidation behavior. Chem Commun 2022;58:6845–8.
[6] Amin M, Shah HH, Fareed AG, Khan WU, Chung E, Zia A, et al. Hydrogen production through renewable and non-renewable energy processes and their impact on climate change. Int J Hydrogen Energy 2022;47:33112–34.
[7] Sarkar B, Barman BK, Nanda KK. Non-precious bimetallic CoCr nanostructures entrapped in bamboo-like nitrogen-

doped graphene tube as a robust bifunctional electrocatalyst for total water splitting. ACS Appl Energy Mater 2018;1:1116–26.
[8] Yuan S, Duan X, Liu J, Ye Y, Lv F, Liu T, et al. Recent progress on transition metal oxides as advanced materials for energy conversion and storage. Energy Storage Mater 2021;42:317–69.
[9] Tang W, Jian J, Chen G, Bian W, Yu J, Wang H, et al. Carbon nanotube supported amorphous MoS2 via microwave heating synthesis for enhanced performance of hydrogen evolution reaction. Energy Mater Adv 2021;2021:1–8.
[10] Liu Q, Sun S, Zhang L, Luo Y, Yang Q, Dong K, et al. N, O-doped carbon foam as metal-free electrocatalyst for efficient hydrogen production from seawater. Nano Res 2022;15:8922–7.
[11] Gao F, He J, Wang H, Lin J, Chen R, Yi K, et al. Te-mediated electro-driven oxygen evolution reaction. Nano Res Energy 2022;1:e9120029.
[12] Qiu Y, Liu Z, Yang Q, Zhang X, Liu J, Liu M, et al. Atmospheric-temperature chain reaction towards ultrathin non-crystal-phase construction for highly efficient water splitting. Chem Eur J 2022;28:e202200683.
[13] You B, Sun Y. Innovative strategies for electrocatalytic water splitting. Acc Chem Res 2018;51:1571–80.
[14] Wang H, Zhou M, Choudhury P, Luo H. Perovskite oxides as bifunctional oxygen electrocatalysts for oxygen evolution/reduction reactions – a mini review. Appl Mater Today 2019;16:56–71.
[15] Ye C, Zhang L, Yue L, Deng B, Cao Y, Liu Q, et al. A NiCo LDH nanosheet array on graphite felt: an efficient 3D electrocatalyst for the oxygen evolution reaction in alkaline media. Inorg Chem Front 2021;8:3162–6.
[16] Qiu Y, Liu Z, Zhang X, Sun A, Ji X, Liu J. Controllable atom implantation for achieving Coulomb-force unbalance toward lattice distortion and vacancy construction for accelerated water splitting. J Colloid Interface Sci 2022;610:194–201.
[17] Xie J, Gao L, Cao S, Liu W, Lei F, Hao P, et al. Copper-incorporated hierarchical wire-on-sheet α-Ni(OH)2 nanoarrays as robust trifunctional catalysts for synergistic hydrogen generation and urea oxidation. J Mater Chem A 2019;7:13577–84.
[18] Audichon T, Napporn TW, Canaff C, Morais C, Comminges C, Kokoh KB. IrO2 coated on RuO2 as efficient and stable electroactive nanocatalysts for electrochemical water splitting. J Phys Chem C 2016;120:2562–73.
[19] Cherevko S, Geiger S, Kasian O, Kulyk N, Grote J-P, Savan A, et al. Oxygen and hydrogen evolution reactions on Ru, RuO2 , Ir, and IrO2 thin film electrodes in acidic and alkaline electrolytes: a comparative study on activity and stability. Catal Today 2016;262:170–80.
[20] Yoo H, Oh K, Lee YR, Row KH, Lee G, Choi J. Simultaneous co-doping of RuO2 and IrO2 into anodic TiO2 nanotubes: a binary catalyst for electrochemical water splitting. Int J Hydrogen Energy 2017;42:6657–64.
[21] Chen D, Chen C, Baiyee ZM, Shao Z, Ciucci F. Nonstoichiometric oxides as low-cost and highly-efficient oxygen reduction/evolution catalysts for low-temperature electrochemical devices. Chem Rev 2015;115:9869–921.
[22] Jamesh M-I, Sun X. Recent progress on earth abundant electrocatalysts for oxygen evolution reaction (OER) in alkaline medium to achieve efficient water splitting – a review. J Power Sources 2018;400:31–68.
[23] Zhou C, Han X, Zhu F, Zhang X, Lu Y, Lang J, et al. Facile synthesis of the encapsulation of Co-based multimetallic alloys/oxide nanoparticles nitrogen-doped carbon nanotubes as electrocatalysts for the HER/OER. Int J Hydrogen Energy 2022;47:27775–86.
[24] Li Z, Wu X, Jiang X, Shen B, Teng Z, Sun D, et al. Surface carbon layer controllable Ni3Fe particles confined in hierarchical N-doped carbon framework boosting oxygen evolution reaction. Adv Powder Mater 2022;1:100020.
[25] Suen NT, Hung SF, Quan Q, Zhang N, Xu YJ, Chen HM. Electrocatalysis for the oxygen evolution reaction: recent development and future perspectives. Chem Soc Rev 2017;46:337–65.
[26] Thangasamy P, Oh S, Nam S, Randriamahazaka H, Oh IK. Ferrocene-Incorporated cobalt sulfide nanoarchitecture for superior oxygen evolution reaction. Small 2020;16:2001665.
[27] Gao L, Cui X, Sewell CD, Li J, Lin Z. Recent advances in activating surface reconstruction for the high-efficiency oxygen evolution reaction. Chem Soc Rev 2021;50:8428–69.
[28] Tiwari AP, Kim D, Kim Y, Lee H. Bifunctional oxygen electrocatalysis through chemical bonding of transition metal chalcogenides on conductive carbons. Adv Energy Mater 2017;7:1602217.
[29] Stevens MB, Trang CDM, Enman LJ, Deng J, Boettcher SW. Reactive Fe-sites in Ni/Fe (Oxy)hydroxide are responsible for exceptional oxygen electrocatalysis activity. J Am Chem Soc 2017;139:11361–4.
[30] Badreldin A, Abusrafa AE, Abdel-Wahab A. Oxygen-deficient cobalt-based oxides for electrocatalytic water splitting. ChemSusChem 2021;14:10–32.
[31] Han H, Qiu Y, Zhang H, Bi T, Yang Q, Liu M, et al. Lattice-disorder layer generation from liquid processing at room temperature with boosted nanointerface exposure toward water splitting. Sustain Energy Fuels 2022;6:3008–13.
[32] Li S, Hao X, Abudula A, Guan G. Nanostructured Co-based bifunctional electrocatalysts for energy conversion and storage: current status and perspectives. J Mater Chem A 2019;7:18674–707.
[33] Hyun S, Ahilan V, Kim H, Shanmugam S. The influence of Co3V2O8 morphology on the oxygen evolution reaction activity and stability. Electrochem Commun 2016;63:44–7.
[34] Pasquini C, Liu S, Chernev P, Gonzalez-Flores D, Mohammadi MR, Kubella P, et al. Operando tracking of oxidation-state changes by coupling electrochemistry with time-resolved X-ray absorption spectroscopy demonstrated for water oxidation by a cobalt-based catalyst film. Anal Bioanal Chem 2021;413:5395–408.
[35] Liu K, Zhu Z, Jiang M, Li L, Ding L, Li M, et al. Boosting electrocatalytic oxygen evolution over Ce–Co9S8 core–shell nanoneedle arrays by electronic and architectural dual engineering. Chem Eur J 2022;28:e202200664.
[36] Li R, Hu B, Yu T, Chen H, Wang Y, Song S. Insights into correlation among surface-structure-activity of cobalt-derived pre-catalyst for oxygen evolution reaction. Adv Sci 2020;7:1902830.
[37] Fan R-Y, Xie J-Y, Yu N, Chai Y-M, Dong B. Interface design and composition regulation of cobalt-based electrocatalysts for oxygen evolution reaction. Int J Hydrogen Energy 2022;47:10547–72.
[38] Yang S, Xie M, Chen L, Wei W, Lv X, Xu Y, et al. Cobalt phosphide nanoparticles embedded in 3D N-doped porous carbon for efficient hydrogen and oxygen evolution reactions. Int J Hydrogen Energy 2019;44:4543–52.
[39] Li M, Wu X, Liu K, Zhang Y, Jiang X, Sun D, et al. Nitrogen vacancies enriched Ce-doped Ni3N hierarchical nanosheets triggering highly-efficient urea oxidation reaction in urea-assisted energy-saving electrolysis. J Energy Chem 2022;69:506–15.
[40] Li J, Wang S, Chang J, Feng L. A review of Ni based powder catalyst for urea oxidation in assisting water splitting reaction. Adv Powder Mater 2022;1:100030.
[41] Yang X, Kang L, Wei Z, Lou S, Lei F, Hao P, et al. A self-sacrificial templated route to fabricate CuFe Prussian blue analogue/Cu(OH)2 nanoarray as an efficient pre-catalyst for

Please cite this article as: He R et al., Accelerate oxygen evolution reaction by adding chemical mediator and utilizing solar energy, International Journal of Hydrogen Energy, https://doi.org/10.1016/j.ijhydene.2022.11.294

ultrastable bifunctional electro-oxidation. Chem Eng J 2021;422:130139.
[42] Sun W, Li J, Gao W, Kang L, Lei F, Xie J. Recent advances in the pre-oxidation process in electrocatalytic urea oxidation reactions. Chem Commun 2022;58:2430–42.
[43] Cassani A, Tuleushova N, Wang Q, Guesmi H, Bonniol V, Cambedouzou J, et al. Fe-modified Pd as an effective multifunctional electrocatalyst for catalytic oxygen reduction and glycerol oxidation reactions in alkaline media. ACS Appl Energy Mater 2021;4:9944–60.
[44] Wan H, Dai C, Jin L, Luo S, Meng F, Chen G, et al. Electro-oxidation of glycerol to high-value-added C1-C3 products by iron-substituted spinel zinc cobalt oxides. ACS Appl Mater Interfaces 2022;14:14293–301.
[45] Fan L, Liu B, Liu X, Senthilkumar N, Wang G, Wen Z. Recent progress in electrocatalytic glycerol oxidation. Energy Technol 2020;9:2000804.
[46] Inoue H, Kimura S, Teraoka Y, Chiku M, Higuchi E, Lam BTX. Mechanism of glycerol oxidation reaction on silver-modified palladium electrode in alkaline medium. Int J Hydrogen Energy 2018;43:18664–71.
[47] Brix AC, Dreyer M, Koul A, Krebs M, Rabe A, Hagemann U, et al. Structure-performance relationship of LaFe1-xCoxO3 electrocatalysts for oxygen evolution, isopropanol oxidation, and glycerol oxidation. Chemelectrochem 2022;9:e202200092.
[48] Li Y, Wei X, Han S, Chen L, Shi J. MnO2 electrocatalysts coordinating alcohol oxidation for ultra-durable hydrogen and chemical productions in acidic solutions. Angew Chem Int Ed 2021;60:21464–72.
[49] Shinagawa T, Ng MT, Takanabe K. Boosting the performance of the nickel anode in the oxygen evolution reaction by simple electrochemical activation. Angew Chem Int Ed 2017;56:5061–5.
[50] Sayed DM, El-Nagar GA, Sayed SY, El-Anadouli BE, El-Deab MS. Activation/deactivation behavior of nano-NiOx based anodes towards the OER: influence of temperature. Electrochim Acta 2018;276:176–83.
[51] Zhang G, Wang H, Yang J, Zhao Q, Yang L, Tang H, et al. Temperature effect on Co-based catalysts in oxygen evolution reaction. Inorg Chem 2018;57:2766–72.
[52] Lu Z. Operation performance study and numerical analysis of the multi-objective adsorption system driven by low-grade heat of solar energy and industrial waste heat. Sol Energy 2020;199:575–84.
[53] Yang L, Sun H, Wang S, Jiang L, Sun G. A solid state thermogalvanic cell harvesting low-grade thermal energy. Int J Hydrogen Energy 2017;42:25877–81.
[54] Gude Vgn N. Desalination using low-grade heat sources. J Energy Eng 2008;134:95–101.
[55] Vélez F, Segovia JJ, Martín MC, Antolín G, Chejne F, Quijano A. A technical, economical and market review of organic Rankine cycles for the conversion of low-grade heat for power generation. Renew Sustain Energy Rev 2012;16:4175–89.
[56] Zhou W, Wu X-J, Cao X, Huang X, Tan C, Tian J, et al. Ni3S2 nanorods/Ni foam composite electrode with low overpotential for electrocatalytic oxygen evolution. Energy Environ Sci 2013;6:2921.
[57] Chen J, Zhang Z, Li H. Insights into the enhanced Lithium-Ion storage performance of CoSx/Carbon polyhedron hybrid anode. J Electroanal Chem 2022;911:116203.
[58] Kong W, Luan X, Du H, Xia L, Qu F. Enhanced electrocatalytic activity of water oxidation in an alkaline medium via Fe doping in CoS2 nanosheets. Chem Commun 2019;55:2469–72.
[59] Ma X, Zhang W, Deng Y, Zhong C, Hu W, Han X. Phase and composition controlled synthesis of cobalt sulfide hollow nanospheres for electrocatalytic water splitting. Nanoscale 2018;10:4816–24.
[60] Ma B, Guo X, Zhang X, Chen Y, Fan X, Li Y, et al. Intercalated graphite between Ni foam and Ni3S2 nanocrystals for the activity promotion in overall water splitting. Energy Technol 2019;7:1900063.
[61] Wei Z, Sun W, Liu S, Qi J, Kang L, Li J, et al. Lanthanum-doped α-Ni(OH)2 1D-2D-3D hierarchical nanostructures for robust bifunctional electro-oxidation. Particuology 2021;57:104–11.
[62] Du J, Xie A, Zhu S, Xiong Z, Yu X, Yang F, et al. 3D flower-like CoNi2S4/polyaniline with high performance for glycerol electrooxidation in an alkaline medium. New J Chem 2019;43:10366–75.
[63] Houache MSE, Hughes K, Baranova EA. Study on catalyst selection for electrochemical valorization of glycerol. Sustain Energy Fuels 2019;3:1892–915.
[64] Cechanaviciute IA, Bobrowski T, Jambrec D, Krysiak OA, Brix AC, Braun M, et al. Aerosol-based synthesis of multi-metal electrocatalysts for oxygen evolution and glycerol oxidation. Chemelectrochem 2022;9:e202200107.
[65] Fan L, Ji Y, Wang G, Chen J, Chen K, Liu X, et al. High entropy alloy electrocatalytic electrode toward alkaline glycerol valorization coupling with acidic hydrogen production. J Am Chem Soc 2022;144:7224–35.
[66] Ju S, Liu Y, Chen H, Tan F, Yuan A, Li X, et al. In situ surface chemistry engineering of cobalt-sulfide nanosheets for improved oxygen evolution activity. ACS Appl Energy Mater 2019;2:4439–49.
[67] Hu X, Tian X, Lin YW, Wang Z. Nickel foam and stainless steel mesh as electrocatalysts for hydrogen evolution reaction, oxygen evolution reaction and overall water splitting in alkaline media. RSC Adv 2019;9:31563–71.
[68] Li Y, Ge X, Wang L, Liu J, Wang Y, Feng L. A free standing porous Co/Mo architecture as a robust bifunctional catalyst toward water splitting. RSC Adv 2017;7:11568–71.
[69] Flynn JH. Temperature dependence of the rate of reaction in thermal analysis- the Arrhenius equation in condensed phase kinetics. J Therm Anal Calorim 1990;36:1579–93.
[70] Aquilanti V, Mundim KC, Elango M, Kleijn S, Kasai T. Temperature dependence of chemical and biophysical rate processes: phenomenological approach to deviations from Arrhenius law. Chem Phys Lett 2010;498:209–13.
[71] Guo P, Wu Y-X, Lau W-M, Liu H, Liu L-M. CoS nanosheet arrays grown on nickel foam as an excellent OER catalyst. J Alloys Compd 2017;723:772–8.
[72] Zhou M, Weng Q, Zhang X, Wang X, Xue Y, Zeng X, et al. In situ electrochemical formation of core–shell nickel–iron disulfide and oxyhydroxide heterostructured catalysts for a stable oxygen evolution reaction and the associated mechanisms. J Mater Chem A 2017;5:4335–42.
[73] Muhich CL, Ehrhart BD, Al-Shankiti I, Ward BJ, Musgrave CB, Weimer AW. A review and perspective of efficient hydrogen generation via solar thermal water splitting, 5. Wiley Interdiscip Rev Energy Environ; 2016. p. 261–87.

Please cite this article as: He R et al., Accelerate oxygen evolution reaction by adding chemical mediator and utilizing solar energy, International Journal of Hydrogen Energy, https://doi.org/10.1016/j.ijhydene.2022.11.294